

Three-Dimensional Imaging of Plant Organs Using a Simple and Rapid Transparency Technique

Journal:	<i>Plant and Cell Physiology</i>
Manuscript ID	PCP-2015-E-00591.R3
Manuscript Type:	Rapid Paper
Date Submitted by the Author:	29-Jan-2016
Complete List of Authors:	Hasegawa, Junko; Faculty of Science and Technology, Tokyo University of Science, Applied Biological Science Sakamoto, Yuki; Faculty of Science and Technology, Tokyo University of Science, Applied Biological Science Nakagami, Satoru; Kumamoto University, Graduate school of science and technology Aida, Mitsuhiro; Nara Institute of Science and Technology (NAIST), Graduate School of Biological Sciences Sawa, Shinichiro; Kumamoto University, Graduate school of science and technology Matsunaga, Sachihiko; Faculty of Science and Technology, Tokyo University of Science, Applied Biological Science
Keywords:	Clearing method, Deep imaging, 3D imaging, Fluorescent protein, 2,2'-thiodiethanol, Transparency technique

Three-dimensional Imaging of Plant Organs Using a Simple and Rapid Transparency Technique

Running Title: Plant organ imaging using a transparency technique

Corresponding Author: Prof. S. Matsunaga

Department of Applied Biological Science, Faculty of Science and Technology

Tokyo University of Science, 2641 Yamazaki, Noda, Chiba 278-8510, Japan

Tel: +81-4-7124-1501 (ext. 3442)

Fax: +81-4-7123-9767

E-mail: sachi@rs.tus.ac.jp

Subject Area: (11) New methodology

Five color figures and no tables

Four supplementary figures

Three-dimensional Imaging of Plant Organs Using a Simple and Rapid Transparency Technique

Running head: Plant organ imaging using a transparency technique

Junko Hasegawa¹, Yuki Sakamoto¹, Satoru Nakagami², Mitsuhiro Aida³, Shinichiro Sawa², and Sachihito Matsunaga¹

¹ Department of Applied Biological Science, Graduate School of Science and Technology, Tokyo University of Science, Noda, Chiba 278-8510, Japan

² Graduate School of Science and Technology, Kumamoto University, Kumamoto, Kumamoto 860-8555, Japan

³ Graduate School of Biological Sciences, Nara Institute of Science and Technology, Ikoma 630-0192, Japan

Abbreviations: DAPI, 4',6-diamidino-2-phenylindole; GFP, green fluorescent protein; PBS, phosphate buffered saline; TDE, 2,2'-thiodiethanol; tdTomato, tandem dimer tomato; YFP, yellow fluorescent protein

Abstract

Clearing techniques eliminate factors that interfere with microscopic observation, including light scattering and absorption by pigments and cytoplasmic components. The techniques allow fluorescence-based detailed analyses of materials and characterization of the three-dimensional structure of organs. We describe a simple and rapid clearing and imaging method, termed “TOMEI” (Transparent plant Organ Method for Imaging), which enables microscopic observation of intact plant organs. This method involves a clearing reagent containing 2,2'-thiodiethanol. Conveniently, transparent plant organs were prepared within only 3–6 hours. We detected fluorescent stains at a depth of approximately 200 μm using confocal laser scanning microscopy and analyzed fluorescent proteins in internal tissues of transparent organs cleared using TOMEI. We adapted TOMEI for various plant organs of *Arabidopsis thaliana* and *Oryza sativa*, including leaves, flower buds, flower stalks, root and nematode-infected root-knots. We visualized whole leaves of *A. thaliana* from the adaxial epidermis to the abaxial epidermis as well as protoxylem and metaxylem vessels of vascular bundles embedded in spongy mesophyll cells. Inner floral organs were observed in flower buds cleared using TOMEI without the need to prepare sections or remove sepals. Multicolor imaging of fluorescent proteins and dyes and analyses of the three-dimensional structure of plant organs based on optical sections are possible using TOMEI. We analyzed root-knots cleared using TOMEI and revealed that nematodes induce giant cell expansion in a DNA content-dependent manner. The

TOMEI method is applicable to analyze fluorescent proteins and dyes quantitatively with cell morphological characteristics in whole plant organs.

Keywords: Clearing method, Deep imaging, Fluorescent protein, 2,2'-thiodiethanol, Transparency technique

For Peer Review

Introduction

When Robert Hooke first reported the existence of the “cell” in 1665, he could only observe the surface layer of cork tissue using a microscope (Hooke 1665). We can now observe cells at much greater depths because of innovations in microscopy, including the development of fluorescent proteins and stains and improved sample preparation methods (Miyawaki 2013). However, the tissue depths that can be penetrated during fluorescence microscopy are limited by several factors, such as light scattering and absorption by pigments and cytoplasmic components. Several sample preparation methods have been established for detailed analyses of structures deep within samples while ensuring three-dimensional (3D) structures and cell-to-cell connections are maintained. For the visualization of mammalian brains and whole bodies, several reagent-based clearing methods can be used to promote optical penetration (Hama et al. 2011, Erturk et al. 2012, Tainaka et al. 2014, Yang et al. 2014, Ye et al. 2014, Acar et al. 2015, Aoyagi et al. 2015, Costantini et al. 2015). Traditionally, plant tissues have been cleared using Hoyer’s medium mainly during beta-glucuronidase (GUS) staining. However, this clearing method cannot be used to detect fluorescence (Kurihara et al. 2015). In addition, Hoyer’s medium requires care during handling because of its anesthetic effect. Recently, novel clearing methods compatible with fluorescent protein detection in plant tissues have been reported (Littlejohn et al. 2010, Littlejohn and Love 2012, Littlejohn et al. 2014, Warner et al. 2014, Kurihara et al. 2015). The methods described by Warner et al. and Kurihara et al. are time-consuming

(Warner's method: 1–3 weeks; ClearSee: 3–4 days) (Warner et al. 2014, Kurihara et al. 2015), while the method by Littlejohn et al. enables the observation of fluorescent proteins in transparent *Arabidopsis thaliana* leaves in only 10 min by immersing samples in perfluorodecalin and perfluoroperhydrophenanthrene (Littlejohn et al. 2010, Littlejohn and Love 2012, Littlejohn et al. 2014).

However, fluorescent signals can be detected at a depth of 75 μm using this method.

In this study, we developed a novel clearing method termed “Transparent plant Organ Method for Imaging” (TOMEI). This method enables the visualization of fluorescent proteins and stains in transparent tissues. It also requires only 3–6 h of fixation and 2,2'-thiodiethanol (TDE) treatment. We analyzed cell structures in whole plant organs at depths of 200–350 μm without the need to prepare sections. Through multicolor imaging of a root-knot cleared using TOMEI, we successfully analyzed the relationship between DNA content and cell volume in endoreduplicated giant cells.

Results

Deep imaging of plant organs with fluorescent staining using TOMEI-I

We selected TDE as the clearing reagent for plant organs. TDE has been used previously as a nontoxic mounting medium to improve the reflective index in animal samples (Staudt et al. 2007). We stained the first foliage leaves of *A. thaliana* plants with 4',6-diamidino-2-phenylindole (DAPI) using TOMEI-I. After

fixation, TOMEI-I did not change the shape of cleared leaves, but the leaves became completely transparent (Fig. 1A). When cleared leaves were placed onto a grid-lined sheet, the grids were clearly visible (Fig. 1A). The leaves cleared using TOMEI-I were as transparent as leaves prepared using a previously reported method (Warner et al. 2014) that took a week to complete (Supplementary Fig. S1).

The leaves were approximately 100 μm thick and were observed from the adaxial epidermis to the abaxial epidermis using confocal microscopy (Fig. 1C, Supplementary Mov. S1). The nuclei were observable in guard cells in the adaxial and abaxial epidermis of the leaves. In addition, we detected the nuclei of palisade and spongy mesophyll cells and secondary cell walls of vascular tissue vessels. When fixed leaves were stained with DAPI and treated with phosphate-buffered saline (PBS) instead of TDE, the nuclei of guard cells in the abaxial epidermis and secondary cell walls of vessels were not observable (Fig. 1C). Strong autofluorescence was observed from the chlorophyll of chloroplasts in palisade mesophyll cells. However, the intensity of autofluorescence was remarkably reduced in transparent leaves prepared using TOMEI-I (Fig. 1C).

Oryza sativa leaves (approximately 80 μm thick) were stained with SYBR Green I or DAPI using TOMEI-I with 97% TDE incubation for 40 min. TOMEI-I had no influence on the morphology of rice leaves but the leaves became more transparent than untreated fixed leaves (Fig. 1B, Supplementary Fig. S2). Autofluorescence from the cell walls and chloroplasts without staining was also observed (Supplementary

Fig. S3). The cleared leaves were observed from the adaxial epidermis to the abaxial epidermis using confocal microscopy (Fig. 1D, Supplementary Fig. S4, Supplementary Mov. S2). Nuclei in the adaxial and abaxial epidermal cells, bulliform cells, and mesophyll cells were detected (Fig. 1D, Supplementary Fig. S4, Supplementary Mov. S2). The intensity of autofluorescence from chlorophyll of mesophyll cells was low, similar to that of *A. thaliana* cells after TOMEI-I. On the other hand, autofluorescence from the cell walls of the adaxial epidermis in *O. sativa* was stronger than that of *A. thaliana*, which might reflect the differences in cell wall composition of *O. sativa* and *A. thaliana* leaves (Fig. 1D, left) (Yokoyama and Nishitani 2004). The staining intensity of nuclei in vascular bundles and commissural veins was stronger than those of bulliform cells and mesophyll cells, respectively (Fig. 1E). Guard cells, mesophyll cells, and epidermal cells of veins were clearly distinguished by rendering using MorphoGraphX (Fig. 1F) (de Reuille et al. 2015).

Root-knots in *A. thaliana* result from nematode infection (Kiyohara and Sawa, 2012). Morphological analyses of giant cells embedded in root-knots were undertaken using sequential slices. After root-knots stained with DAPI or SYBR Green I were cleared using TOMEI-I, we observed giant cells in a whole root-knot (width: 60 μm) using confocal microscopy (Fig. 2A, B, Supplementary Mov. S3). The optical cross-section of the giant cells revealed the presence of endoreduplicated and multinucleated cells, which suggested cell heterogeneity (Fig. 2B).

After DAPI-stained *A. thaliana* flower stalks were cleared using TOMEI-I, the fluorescence from nuclei and cell walls was detected at a depth of 200 μm by confocal microscopy (Fig. 2C). The three-dimensional (3D) structure of the flower stalk was constructed from 200 optical sections using FluoRender (Wan et al. 2012) (Fig. 2C, Supplementary Mov. S4). The Y–Z (Fig. 2D) and X–Z (Fig. 2E) sections represented longitudinal and transverse sections of vascular bundles, respectively. In addition to epidermal and guard cells (Fig. 2F), protoxylem and metaxylem vessels were clearly observed (Fig. 2G, H). Extended flat nuclei were observed in the optical section at 192 μm depth (Fig. 2I).

We also constructed the 3D structure of a whole flower stalk (width: 350 μm) using two-photon microscopy (Supplementary Fig. S5A, B). The 3D structure provided a 360° view of the epidermal surface and indicated the positions of the inner vascular bundles. We also observed nuclei stained with DAPI in the internal tissues of *A. thaliana* leaf buds using two-photon microscopy, without the need to prepare sections (Supplementary Fig. S5C). We constructed a 3D leaf bud stained with DAPI (Supplementary Fig. S5D). The 3D image of the leaf bud based on optical sections indicated the position of leaf primordia.

Mutant analysis of flower buds with fluorescent staining using TOMEI-I

In phenotypic analyses of flower buds, sepals or petals should be removed or histological sections should be prepared to analyze inner floral organs. However, TOMEI enables analysis of the inner organs of whole

intact flower buds (Fig. 3A). When a stage 9 flower bud cleared using TOMEI-I was observed by confocal microscopy, nuclei of floral organs, including petals, stamens, and the gynoecium, and nuclei and cell walls of sepals were clearly detected through the sepal up to a depth of 180 μm (Fig. 3B, Supplementary Mov. S5). We next applied TOMEI-I to developing gynoecia in young flower buds. In *A. thaliana* plants, the gynoecium primordium is initiated as a tubular structure with its distal end open (Hill and Lord 1989, Roeder and Yanofsky 2006). The open end eventually closes because of post-genital fusion, forming the solid tissue of the style (Nahar et al. 2012). In cleared *A. thaliana* Landsberg *erecta* (*Ler*) samples, the open end of the gynoecium in stage 9 flower buds was clearly visible as a slit in an optical longitudinal section (Fig. 3C, top and middle). Reconstruction of transverse sections from a series of longitudinal sections revealed a specific morphology at the open end, in which the two opposing medial ridges were present on the adaxial side of the gynoecium tube (Fig. 3C, bottom). In the basal region, which gives rise to the ovary, early ovule primordia were observed (Fig. 3C, middle). Importantly, the TOMEI-I method readily enabled detection of these anatomical features in whole floral buds with many other floral organs surrounding the gynoecium primordium. Thus, the method permitted examination of the primordium structure during the early stages of flower development without prior dissection, which is often laborious and technically difficult because of the small size of the buds.

We also analyzed the *cuc2 spt* double mutant, which is defective in gynoecium closure at the distal end

and shows a reduced number of ovules and poor septum development in the ovary (Nahar et al. 2012).

Previous analyses using scanning electron microscopy have shown that the opening at the distal end of the mutant gynoecium is wider than that of the wild-type plant. This phenotype was confirmed in stage 9 gynoecium samples prepared using TOMEI-I (Fig. 3D, top and middle). Reconstructed transverse sections showed smaller medial ridges in the mutant (Fig. 3D, bottom), again confirming the previous observation that the gynoecium closure defect was due to reduced ridge growth (Nahar et al. 2012). Furthermore, we determined for the first time that no visible ovule primordia were present in the *cuc2 spt* gynoecium at this stage (Fig. 3D, middle). This finding may be correlated with the previously reported reduction in the number of mature ovules (Nahar et al. 2012), and further supports the utility of the TOMEI method for observation of internal tissues.

TOMEI-I allows observation of gynoecia at later stages when thicker tissues with more complicated internal structures are present. However, removal of the outer floral organs may be necessary to obtain clear images. In stage 11 and 12 gynoecia of *Ler*, the closed style at the distal end was visible (Fig. 3E), whereas the corresponding style in *cuc2 spt* mutants remained open (Fig. 3F). Ovule primordia were arranged in regular rows in wild-type samples (Fig. 3E), whereas mutant ovule primordia were somewhat irregularly distributed, especially in stage 12 gynoecia (Fig. 3F).

Use of DAPI as a staining reagent reveals nuclear morphology and size, which are important traits

associated with cellular differentiation. In gynoecia at early developmental stages, the nuclei were a uniform size and were mostly round regardless of position within the tissues (Fig. 3C, D). In contrast, nuclear shape and size were variable at later developmental stages (Fig. 3E, F). For example, nuclei within stigmatic papillae cells were elongated and much larger than those of the surrounding cells (Fig. 3G).

Observation of fluorescent proteins in transparent organs prepared using TOMEI-II

For samples fixed with Fixative solution I (acetic acid:ethanol = 1:3) in TOMEI-I, we observed quenching of protein fluorescence, including that of green fluorescent protein (GFP) and *Discosoma* red (dsRed)-derived fluorescent proteins. To prevent quenching, Fixative solution I was replaced with Fixative solution II (4% paraformaldehyde in PBS, pH 7.0) in TOMEI-II. The locations of fluorescent proteins in transparent organs could be determined using TOMEI-II. The first foliage leaves of *A. thaliana* expressing histone H2B fused to the tandem dimer tomato (histone H2B-tdTomato) were stained with Calcofluor White and then treated sequentially with 10%, 30%, 50%, 70%, and 97% TDE solutions. Although the light penetration of the transparent leaves of *A. thaliana* prepared with TOMEI-II was lower than that using TOMEI-I due to incomplete removal of chlorophyll (Fig. 4A), histone H2B-tdTomato in nuclei was observed in the adaxial and abaxial epidermis of the leaves (Fig. 4B, Supplementary Mov. S6). We detected no reduction of tdTomato signal intensity after 72 h treatment (Supplementary Fig. S6). A similar

visualization was achieved in *A. thaliana* leaves expressing histone H2B fused to the yellow fluorescent protein (histone H2B-YFP) (Supplementary Fig. S7), indicating that TOMEI-II could be used with fluorescent proteins derived from coral and jellyfish. The fluorescence of H2B-tdTomato in nuclei and Calcofluor White in cell walls was simultaneously observed in transparent leaves (Fig. 4C). The nuclei were visualized in pavement cells of the epidermis, palisade and spongy mesophyll cells, and vascular cells. Nuclei treated with DAPI and cell membranes in plants expressing H2B-GFP and LTI6b-tdTomato were visualized to provide a 360° view of the whole root (Supplementary Fig. S8). TOMEI-II with 20% TDE was enough to analyze the whole root of *A. thaliana* because the root is natively transparent. In *A. thaliana* root-knots, H2B-GFP and LTI6b-tdTomato were simultaneously detected (Fig. 4D, E). The 3D structure (width: 118 μm), which was constructed from 118 optical sections using FluoRender, revealed that the giant cells consisted of endoreduplicated and multinucleated cells.

Relationship between amount of DNA and cell volume in giant cells

Nematodes inject effector proteins into the cells of root vascular tissues (de Almeida Engler and Gheysen 2013). Endoreduplication and multinucleation are induced in the affected cells, leading to an increase in cell volume and the development of giant cells (de Almeida Engler and Gheysen 2013; Rodiuc et al. 2014). To characterize the relationship between DNA content and cell volume in giant cells, we inoculated *A.*

thaliana Columbia-0 (Col-0) roots with *Meloidogyne incognita* nematodes. The infected roots were fixed, stained, and cleared using TOMEI-II 6 and 7 days post-infection. We measured the amount of DNA in endoreduplicated or multinucleated cells and giant cell volumes using 3D structures constructed from confocal images of samples stained with histone H2B-GFP/LTI6b-tdTomato line (Fig. 4D, E) and Calcofluor White and SYBR Green I (Fig. 5A). A strong positive correlation between DNA amount and cell volume, based on data derived from fluorescent proteins and dyes, was observed in giant cells (Fig. 5B, Supplementary Fig. S9). This result suggests that increase in giant cell volume is correlated with increase in DNA amount.

Discussion

The novel clearing procedure, TOMEI, has considerable advantages over established methods for investigations of plant organs. A clearing method used for animal organs that included reagents containing urea, sugar alcohol and detergent (Hama et al. 2011) was adapted for use with plant organs (Warner et al. 2014, Kurihara et al. 2015). Warner et al. method and ClearSee permit simultaneous observation of fluorescent proteins and stains, but sample preparation requires 1–3 weeks or 3–4 days, respectively. The novel method TOMEI can be completed in 3–6 h and allows simultaneous detection of fluorescent proteins and dyes, such as Calcofluor White, DAPI, and SYBR Green I, at a depth of 200 μm using confocal

microscopy. This method thus enables rapid phenotyping of plant organs.

The clearing methods requiring TDE used to prepare fixed animal brains cause brain shrinkage proportional to the TDE concentration. The fixed brain becomes extremely small after 1–2 days of immersion in 97% TDE (Aoyagi et al. 2015). In contrast, treatment with 97% TDE in TOMEI did not result in shrinkage or expansion of plant organs. This tolerance of plant organs to high TDE concentrations may be due to cell wall rigidity. Moreover, high TDE concentrations quench fluorescence in animal cells (Staudt et al. 2007). Therefore, 47% or 60% TDE has been used to avoid decreasing the intensity of fluorescent signals in animal tissues (Aoyagi et al. 2015, Costantini et al. 2015). However, GFP signals can be detected in transparent plant organs prepared using TOMEI-II (with 97% TDE). This is because samples are treated with TDE for a relatively short period (less than 3 h), which minimizes the quenching of fluorescence. In addition, tdTomato signals were not quenched for at least 3 days (Supplementary Figure S6), suggesting that transparent organs treated with TOMEI-II can be observed for several days after preparation.

The nuclei of giant cells in *A. thaliana* root-knots can be visualized in enough detail to enable the determination of cross-sectional area (Vieira et al. 2012, 2013). Nuclei and cell walls were simultaneously observed in giant cells cleared using TOMEI-II. Although the visualization of nuclei (Viera et al. 2012) and measurement of cell volume using serial sections (Cabrera et al. 2015) have been independently described, to our knowledge the simultaneous analysis of DNA content and cell volume has not been reported

previously. The knockdown of *CCS52*, which encodes an endoreduplication enhancer, or overexpression of *KRP4*, which encodes an endoreduplication suppressor, inhibits the growth of giant cells and decreases the number of nematode eggs (de Almeida Engler et al. 2012, Vieira et al. 2012, 2013). These studies suggest that DNA content is correlated with cell volume in giant cells. However, no experimental evidence has proved this proposed correlation. The results of our analyses of cleared giant cells provide the first evidence that DNA content in nuclei is positively correlated with giant cell volume. Nematodes use the increasing amounts of cytoplasmic components in giant cells as a nutrient source (Rodiuc et al. 2015). Nematodes also use a host mechanism to increase plant cell volume, ultimately leading to the formation of giant cells. Although *A. thaliana* cell volumes expand in DNA content-dependent and -independent manners (Melaragno et al. 1993, Sablowski and Dornelas 2013), it was previously unknown whether giant cell formation is associated with DNA content. Our analyses revealed that the increase in giant cell volume is dependent on DNA content. Meristematic cells of *A. thaliana* mainly expand through an increase in cytoplasmic volume, whereas differentiated cells expand through an increase in vacuolar volume in a turgor pressure-driven manner (Sablowski and Dornelas 2013). The giant cell vacuolar volumes increase during early developmental stages and the vacuoles are eventually compartmentalized. Finally, the cytoplasmic volume increases considerably. A high density of cytoplasmic components is preferable over vacuolar expansion because nematodes consume giant cells. Nematodes may supply an inducer of endoreduplication

and multinucleation and a transdifferentiation factor to convert vacuolar expansion to the production of cytoplasmic components during the formation of giant cells.

In conclusion, TOMEI is a powerful tool for three-dimensional imaging of plant organs at single-cell resolution and in-depth imaging of plant cell morphology that enables observation of thick organs in 3-6 hours. TOMEI will contribute to rapid phenotyping in various plant developmental phenomena, including growth and development, fertilization, environmental response and plant-microbe or -parasite interactions.

Materials and Methods

Plant materials

Arabidopsis thaliana Columbia-0 (Col-0) plants and transgenic plants carrying the following constructs were used: proCaMV35S::H2B-YFP, proRPS5a::H2B-tdTomato (Adachi et al. 2011), and proRPS5a::H2B-GFP/ proRPS5a:: tdTomato-LTI6b (Mizuta et al. 2015). To construct vectors of histone H2B fused with the fluorescent protein, histone H2B gene (HTB1; At1g07790) and histone H2B CDS (HTB2; At5g22880) were amplified by PCR and cloned into the pENTR™/D-TOPO® vector (Thermo Fisher Scientific) using the TOPO® cloning method and into the pENTR 1A vector (Thermo Fisher Scientific) by In-Fusion® HD Cloning Kit (Clontech), and transferred to the pGWB504 or pGWB541 binary vectors (Tanaka et al. 2011) by Gateway® Technology (Thermo Fisher Scientific). Transformation

of *A. thaliana* Col-0 was performed by the floral dip method with *Agrobacterium tumefaciens*.

Seeds were sterilized in 70% ethanol for 5 min and 10% sodium hypochlorite supplemented with 0.01% Triton X-100 for 15 min. Seeds were washed twice in sterilized water and sowed on half-strength Murashige and Skoog (MS) medium (half-strength MS salt mixture, 1% sucrose, and 1% gellan gum), pH 5.8 (adjusted with KOH). The seeds were incubated at 4 °C for 1 day and the seedlings grown at 22 °C with a 16 h light/8 h dark cycle. Flower buds of Col-0 plants grown on rockwool at 22 °C with a 16 h light/8 h dark cycle were used. Flower buds from *A. thaliana* Landsberg *erecta* (*Ler*) and *cuc2 spt* plants were collected as previously described (Kamiuchi et al. 2014). *Oryza sativa* L. 'Nipponbare' seeds were sterilized in 10% sodium hypochlorite for 20 min and washed five times with water. Seeds were germinated in water and grown at 25 °C under continuous light. We used 2-week-old plants for subsequent experiments.

Nematode preparation and inoculation

Solanum lycopersicum 'Pritz' tomato plants were inoculated with *M. incognita* as described previously (https://www.plantcellwall.jp/protocol/pdf/protocol_1.pdf). Briefly, 6- to 7-week-old tomato seedlings were inoculated at 3-day intervals for a total of four inoculations. Approximately 80,000 second-stage juveniles (J2) were applied to each plant. The inoculated tomato plants were transferred to a hydroponic system, and

after 2- to 4-day intervals, J2 nematodes were collected. The *A. thaliana* plants were grown vertically on plates containing 1/4 MS salt mixture, 0.5 % sucrose, and 0.6 % phytigel, pH 6.4, under continuous light at 22 °C. We inoculated 5-day-old seedlings with approximately 80 J2 nematodes. Plants were then grown at 22 °C with a 16 h light/8 h dark cycle for 6 or 7 days.

TOMEI-I

Plant organs were steeped in Fixative solution I (acetic acid:ethanol = 1:3) for 1–2 h. After washing with 70% ethanol and immersion in PBS, the samples were stained with DAPI or SYBR Green I. Finally, the samples were immersed in TDE solution, which contained 147 µM *n*-gallic acid in PBS and 97% TDE (Sigma). TDE solution was stored at 4 °C. Samples cleared using TOMEI-I can be stored for at least 1 week at 4 °C.

DAPI staining of A. thaliana first foliage leaves, flower buds, and flower stalks by TOMEI-I

The first foliage leaves from 30-day-old *A. thaliana* plants, flower buds, and flower stalks were treated with Fixative solution I for 1 or 2 h at 25 °C. The duration of fixation depended on sample thickness. The samples were washed in 70% ethanol for 10 min and then PBS for 5 min at 25 °C. The leaves were stained with 5 µg/ml DAPI in PBS for 5 min and other organs were stained with 10 µg/ml DAPI in PBS for 30 min

and then washed three times in PBS for 8 min. Finally, the leaves were treated with 97% TDE for 20 min at 25 °C.

DAPI and SYBR Green I staining of O. sativa leaves by TOMEI-I

Two-week-old *O. sativa* leaves were treated with Fixative solution I for 1 h at 25 °C. The leaves were washed in 70% ethanol for 10 min, and then PBS for 10 min at 25 °C. The leaves were stained with SYBR Green I (Thermo Fisher Scientific) (diluted 1:2000 with PBS) or 10 µg/ml DAPI in PBS for 30 min. The stained leaves were washed three times in PBS for 8 min and treated with 97% TDE for 20 min at 25 °C.

TOMEI-II

To avoid the quenching of protein fluorescence by Fixative solution I, the samples were evaporated in Fixative solution II (4% paraformaldehyde in PBS, pH 7.0), incubated for 1 h at 25 °C, and washed three times in PBS. Washed samples were incubated in TDE supplemented with *n*-gallic acid. Fixed samples were stored in PBS at 4 °C for at least 1 week before the TDE procedure if immediate observation after sample preparation was not possible.

Observation of fluorescent proteins and stain in A. thaliana root-knots and leaf buds by TOMEI-II

Root-knots and 3-day-old seedlings were treated with Fixative solution II for 1 h at 25 °C and washed twice in PBS for 10 min. Samples were treated twice with PEMT buffer (50 mM PIPES [pH 6.8], 2 mM EGTA [pH 7.0], 2 mM MgSO₄, and 0.5% [v/v] Triton X-100) for 15 min and stained for 10 min with 10 µg/ml DAPI in PBS or 1:2000 SYBR Green I. The stained leaves were washed three times with PBS for 10 min. For cell wall staining, the leaves were treated with Calcofluor White Stain (Fluka) for 10 min at 25 °C and washed twice in PBS. The root-knots were treated in 97% TDE supplemented with *n*-gallic acid for 5–20 min depending on root-knot thickness.

Observation of fluorescent proteins in A. thaliana leaves by TOMEI-II

The leaves were evaporated in Fixative solution II, incubated for 1 h at 25 °C, and washed three times in PBS. For cell wall staining, leaves were treated with Calcofluor White Stain for 10 min at 25 °C and washed twice in PBS. The leaves were treated sequentially with 10%, 30%, 50%, 70%, and 97% TDE in PBS for 10 min at 25 °C on glass microscope slides. Finally, the samples were incubated in 97% TDE for 1 h at 25 °C.

Observation of fluorescent proteins and stain in A. thaliana roots by TOMEI-II

Roots were treated with Fixative solution II for 1 h at 25 °C and washed twice in PBS for 10 min. The roots

were treated twice with PEMT buffer for 15 min and then stained with a mixture of DAPI solution (CyStainUV Precise P, PARTEC) and PBS (1:3) for 3 min. The stained samples were mounted in 20% TDE supplemented with *n*-gallic acid.

Microscopy

Samples were observed with a confocal laser microscope (FV1000, Olympus), which included the Olympus FV 10-MCPSU (405 nm) and 40 × 0.95 N.A. dry objective (UPlanSApo, Olympus). We also used a spinning disc confocal laser microscope (IX 81, Olympus), which included the Xe laser (405 nm, 488 nm, and 561 nm) in a confocal spinning unit (CSU-X1, Yokogawa), 20 × 0.85 N.A. oil immersion objective (UPlanSApo, Olympus), 40 × 1.3 N.A. oil immersion objective (UPlanFLN, Olympus) with a working distance of 200 μm, 60 × 1.4 N.A. oil immersion objective (PlanApo, Olympus), and sCMOS camera (Neo 5.5 sCMOS, ANDOR or Zyla 4.2 plus sCMOS, ANROR). A two-photon excitation microscope (FVMPE-RS, Olympus) equipped with the In Sight DS-OL laser (750 nm) and 25 × 1.00 N.A. glycerol immersion objective (XLSLPlanN, Olympus) was also used. All z-sections were collected at 1 μm intervals.

Image processing and analysis

Images were rendered and analyzed with the following software: ImageJ (Schneider et al. 2012), FluoRender (Wan et al. 2012), Fluoview (FV10-ASW4.2, Olympus), MorphoGraphX (de Reuille et al. 2015), and MetaMorph (Molecular Devices). We manually traced the outline of giant cells and nuclei in all optical sections and measured cell volumes and DNA amounts using ImageJ. Statistical analysis was performed with R version 3.2.0 (R Development Core Team 2015). The intensity of fluorescence signals was measured using ImageJ. The C value based on the fluorescence intensity of H2B-GFP or SYBR Green I was calculated using the fluorescence of nuclei with 2C in the meristematic region of roots as a standard.

Funding

This work was supported by CREST grants from the Japan Science and Technology Agency to S.M.; MXT/JSPS KAKENHI to S.M.; and a grant from the JSPS Research Fellowships for Young Scientists to J.H.

Disclosures

The authors have no conflicts of interest to declare.

Acknowledgments

We thank Drs. Hiroyuki Tsuji and Mika Tsugane for valuable comments regarding *O. sativa* tissues, Dr. Natsumaro Kutsuna for advice about imaging analysis, Ms. Miyuki Kohmura for advice about two photon microscopy, Ms. Yukiko Kawaguchi for coloring the 3D structures and Dr. Daisuke Kurihara for giving proRPS5a:: tdTomato-LTI6b vector.

References

Acar, M., Kocherlakota, K.S., Murphy, M.M., Peyer, J.G., Oguro, H., Inra, C.N., et al. (2015) Deep imaging of bone marrow shows non-dividing stem cells are mainly perisinusoidal. *Nature* 526: 126–130.

Adachi, S., Minamisawa, K., Okushima, Y., Inagaki, S., Yoshiyama, K., Kondou, et al. (2011) Programmed induction of endoreduplication by DNA double-strand breaks in Arabidopsis. *Proc. Natl. Acad. Sci. USA* 108: 10004–10009.

de Almeida Engler, J., Kyndt, T., Vieira, P., Van Cappelle, E., Boudolf, V., Sanchez, V., et al. (2012) CCS52 and DEL1 genes are key components of the endocycle in nematode-induced feeding sites. *Plant J.* 72: 185–198.

de Almeida Engler, J. and Gheysen, G. (2013) Nematode-induced endoreduplication in plant host cells: why and how? *Mol. Plant-Microbe Interact.* 26(1): 17–24.

Aoyagi, Y., Kawakami, R., Osanai, H., Hibi, T., and Nemoto, T. (2015) A rapid optical clearing protocol using 2,2-thiodiethanol for microscopic observation of fixed mouse brain. *PLoS ONE*. 10(1): e0116280.

de Reuille, P.B., Routier-Kierzkowska, A.L., Kierzkowski, D., Bassel, G.W., Schüpbach, T., Tauriello, G. et al. (2015) MorphoGraphX: A platform for quantifying morphogenesis in 4D. *eLife* 4: 05864.

Cabrera, J., Diaz-Manzano, F.E., Barcala, M., Arganda-Carreras, I., de Almeida-Engler, J., Engler, G., et al.

(2015) Phenotyping nematode feeding sites: three-dimensional reconstruction and volumetric measurements of giant cells induced by root-knot nematodes in *Arabidopsis*. *New Phytol.* 206: 868-880.

Costantini, I., Ghobril, J.P., Di Giovanna, A.P., Allegra Mascaro, A.L., Silvestri, L., Müllenbroich, M.C., et al. (2015) A versatile clearing agent for multi-modal brain imaging. *Sci. Rep.* 5: 9808.

Erturk, A., Mauch, C.P., Hellal, F., Forstner, F., Keck, T., Becker, K., et al. (2012) Three-dimensional imaging of the unsectioned adult spinal cord to assess axon regeneration and glial responses after injury. *Nat. Med.* 18: 166-171.

Hama, H., Kurokawa, H., Kawano, H., Ando, R., Shimogori, T., Noda, H., et al. (2011) Scale: a chemical approach for fluorescence imaging and reconstruction of transparent mouse brain. *Nat. Neurosci.* 14: 1481-1488.

Hill, J. P. and Lord, E. M. (1989) Floral development in *Arabidopsis thaliana*: a comparison of the wild type and the homeotic *pistillata* mutant. *Can. J. Bot.* 67: 2922-2936.

Hooke, R. (1665) *Micrographia: Or Some Physiological Descriptions of Minute Bodies Made by Magnifying Glasses, with Observations and Inquiries Thereupon.* p. 113. Courier Dover Publications, New York

Jegu, T., Latrasse, D., Delarue, M., Mazubert, C., Bourge, M., Hudik, E., et al. (2013) Multiple functions of Kip-related protein5 connect endoreduplication and cell elongation. *Plant Physiol.* 161(4): 1694-1705.

Kamiuchi, Y., Yamamoto, K., Furutani, M., Tasaka, M. and Aida, M. (2014) The CUC1 and CUC2 genes promote carpel margin meristem formation during *Arabidopsis* gynoecium development. *Front. Plant Sci.* 5:165.

Kiyohara, S., Sawa, S. (2012) CLE signaling systems during plant development and nematode infection. *Plant Cell Physiol.* 53(12):1989-1999

Kurihara, D., Mizuta, Y., Sato, Y., Higashiyama, T. (2015) ClearSee: a rapid optical clearing reagent for whole-plant fluorescence imaging. *Development*. 142(23): 4168-4179.

Littlejohn, G.R., Gouveia, J.D., Edner, C., Smirnoff, N., and Love, J. (2010) Perfluorodecalin enhances in vivo confocal microscopy resolution of *Arabidopsis thaliana* mesophyll. *New Phytol.* 186: 1018-1025.

Littlejohn, G.R. and Love, J. (2012) A simple method for imaging *Arabidopsis* leaves using perfluorodecalin as an infiltrative imaging medium. *J. Vis. Exp.* 16: (59).

Littlejohn, G.R., Mansfield, J.C., Christmas, J.T., Witterick, E., Fricker, M.D., Grant, M.R., et al. (2014) An update: improvements in imaging perfluorocarbon-mounted plant leaves with implications for studies of plant pathology, physiology, development and cell biology. *Front Plant Sci.* 5:140.

Melaragno, J.E., Mehrotra, B., and Coleman, A.W. (1993) Relationship between Endopolyploidy and Cell Size in Epidermal Tissue of *Arabidopsis*. *Plant Cell*. 5: 1661-1668.

Miyawaki, A. (2013) Fluorescence imaging in the last two decades. *Microscopy*. 62(1): 63-68.

Mizuta, Y., Kurihara, D., Higashiyama, T. (2015) Two-photon imaging with longer wavelength excitation in intact *Arabidopsis* tissues. *Protoplasma*. 252(5):1231-1240.

Nahar, M.A, Ishida, T., Smyth, D.R., Tasaka, M. and Aida, M. (2012) Interactions of *CUP-SHAPED COTYLEDON* and *SPATULA* genes control carpel margin development in *Arabidopsis thaliana*. *Plant Cell Physiol.* 53: 1134-1143

Sablowski, R., and Carnier Dornelas, M. (2014) Interplay between cell growth and cell cycle in plants. *J.Exp. Bot.* 65(19):2703-2714

Schneider, C.A., Rasband, W.S., Eliceiri, K.W. (2012) "NIH Image to ImageJ: 25 years of image analysis". *Nature Methods* 9, 671-675.

Staudt, T., Lang, M.C., Medda, R., Engelhardt, J., and Hell, S.W. (2007) 2,2'-thiodiethanol: a new water soluble mounting medium for high resolution optical microscopy. *Microsc. Res. Tech.* 70: 1-9.

R Development Core Team 2015, R: A language and environment for statistical computing. R Foundation for Statistical Computing, Vienna, Austria. <http://www.R-project.org/>.)

Rodiuc, N., Vieira, P., Banora, M.Y. and de Almeida Engler, J. (2014) On the track of transfer cell formation by specialized plant-parasitic nematodes. *Front. Plant Sci.* 5:160.

Roeder, A.H.K. and Yanofsky, M.F. (2006) Fruit development in *Arabidopsis*. *Arabidopsis Book* .4: e0075.

Tainaka, K., Kubota, S.I., Suyama, T.Q., Susaki, E.A., Perrin, D., Ukai-Tadenuma, M., et al. (2014) Whole-body imaging with single-cell resolution by tissue decolorization. *Cell*. 159: 911-924.

Schneider, C.A., Rasband, W.S. and Eliceiri, K.W. (2012) NIH Image to ImageJ: 25 years of image analysis. *Nat. Methods*. 9: 671-675

Tanaka, Y., Nakamura, S., Kawamukai, M., Koizumi, N., Nakagawa, T. (2011) Development of a series of gateway binary vectors possessing a tunicamycin resistance gene as a marker for the transformation of *Arabidopsis thaliana*. *Biosci Biotechnol Biochem.* 75(4):804-807.

Vieira, P., Engler, G., and de Almeida Engler, J. (2012) Whole-mount confocal imaging of nuclei in giant feeding cells induced by root-knot nematodes in *Arabidopsis*. *New Phytol.* 195: 488-496.

Vieira, P., Escudero, C., Rodiuc, N., Boruc, J., Russinova, E., Glab, N., et al. (2013) Ectopic expression of Kip-related proteins restrains root-knot nematode-feeding site expansion. *New Phytol.* (2):505-519.

Wan, Y., Otsuna, H., Chien, C.B. and Hansen, C. (2012) FluoRender: An Application of 2D Image Space Methods for 3D and 4D Confocal Microscopy Data Visualization in Neurobiology Research. *IEEE Pac. Vis.*

Symp. 201-208.

Warner, C.A., Biedrzycki, M.L., Jacobs, S.S., Wisser, R.J., Caplan, J.L., and Sherrier, D.J. (2014) An optical clearing technique for plant tissues allowing deep imaging and compatible with fluorescence microscopy. *Plant Physiol.* 166: 1684-1687.

Yang, B., Treweek, J.B., Kulkarni, R.P., Deverman, B.E., Chen, C.K., Lubeck, E., et al. (2014) Single-Cell Phenotyping within Transparent Intact Tissue through Whole-Body Clearing. *Cell.* 158: 945-958.

Ye, R.T., Hsueh, B., and Deisseroth, K. (2014) Advanced CLARITY for rapid and high-resolution imaging of intact tissues. *Nat. Protoc.* 9: 1682-1697.

Legends to figures

Fig. 1 Imaging of *A. thaliana* and *O. sativa* leaves cleared using TOMEI. Images of *A. thaliana* first foliage leaf (A) and *O. sativa* leaf blade (B) before and after TOMEI-I treatment. The left, middle, and right panels show untreated, fixed and TOMEI-I-treated leaves, respectively. A magenta dashed line (A) indicates the leaf outline. Each small square on the grid corresponds to 1 mm². (C) *A. thaliana* first foliage leaves stained with DAPI were observed using confocal microscopy. The first foliage leaves were treated with PBS after fixation (upper panels) or cleared using TOMEI-I (lower panels). Confocal optical sections were arranged from the adaxial surface to the abaxial surface. (D, E) *Oryza sativa* leaf blade stained with SYBR Green I observed from the adaxial surface to the abaxial surface using confocal microscopy. (F) The confocal images of the leaf blade were used to construct a three-dimensional image with MorphoGraphX. Nuclei of

guard cells, mesophyll cells, and epidermal cells are colored blue, pink, and yellow, respectively. Green represents autofluorescence from cell walls. Dashed lines show each axis: blue, X-axis; orange, Y-axis; green, Z-axis. Pink arrows indicate guard cells (C, D). Green and yellow arrowheads indicate vascular tissue and commissural veins, respectively (D, E). Scale bars correspond to 50 μm (C,D), 25 μm (E).

Fig. 2 Imaging of *A. thaliana* root-knots and flower stalks cleared using TOMEI. (A–H) Nuclei and cell walls in each tissue were stained with DAPI or SYBR Green I. (A, B) A root-knot induced by *Meloidogyne incognita* infection was stained with SYBR Green I. (A) Serial optical sections from the epidermis to the internal tissue of a root-knot. Scale bar corresponds to 50 μm . (B) Maximum-intensity projection image of cleared giant cells from five optical sections. Magenta arrowheads indicate nuclei in giant cells and blue dashed lines indicate the outline of giant cells. Scale bar corresponds to 50 μm . (C) Three-dimensional (3D) image of a flower stalk cleared using TOMEI-I. The confocal images were used to construct the 3D image with FluoRender. Dashed lines show each axis: blue, X-axis; orange, Y-axis; green, Z-axis. (D) Maximum-intensity projection image of the Z–Y plane. (E) Maximum-intensity projection image of the Z–X plane. 0, 100 and 200 μm indicate the depth from the epidermis of the flower stalk. Arrowheads indicate vascular vessels. (F) Single optical section of the epidermis of the cleared flower stalk. Scale bar corresponds to 25 μm . (G) Projection image of metaxylem in the cleared flower stalk. (H)

Maximum-intensity projection image of protoxylem in the cleared flower stalk. Scale bar corresponds to 5 μm . (I) The image in 192 μm in depth in flower stalk. Arrowheads indicate nuclei. Scale bar corresponds to 50 μm .

Fig. 3 Imaging of *A. thaliana* flower buds cleared using TOMEI. (A) Images of the flower buds before (left) and after TOMEI-I treatment (right). Each small square on the grid corresponds to 1 mm^2 . (B–G) Cleared stage 9 flower buds from *A. thaliana* ‘Columbia-0’ (Col-0) stained with DAPI were observed from the sepals to the gynoecium using confocal microscopy. (B) The upper panels are serial optical sections of a whole Col-0 flower bud. The lower panels present magnified images of the floral organs. The arrowhead indicates a vascular vein and the dotted line indicates the outline of a petal. Se, sepal; Pe, petal; St, stamen; Pi, pistil. (C) Cleared stage 9 flower buds from *A. thaliana* Landsberg *erecta* (*Ler*) and (D) the *cuc2 spt* mutant. (Top) Longitudinal optical section of a whole flower bud. (Middle) Magnified view of the distal half of a gynoecium primordium. Blue arrows and pink arrowheads indicate a slit at the distal end and an ovule primordium in the basal part, respectively. (Bottom) Transverse section reconstructed from serial longitudinal sections. Asterisks indicate the positions of medial ridges. Scale bars correspond to 100 μm (upper) and 50 μm (middle). Cleared gynoecia of *Ler* (E) and the *cuc2 spt* mutant (F) taken from stage 12 flower buds. Arrowheads indicate ovule primordia. Sty, style; o, ovary. Scale bar corresponds to 50 μm . (G)

Magnified view of the distal end of a *Ler* gynoecium at stage 12. The dotted line indicates the border between stigmatic papillae cells (Sp) and the style (Sty). Scale bar corresponds to 10 μm .

Fig. 4 Imaging of fluorescent proteins in *A. thaliana* organs cleared using TOMEI. (A) First foliage leaves were untreated (left) and cleared using TOMEI-II (right). Each small square on the grid corresponds to 1 mm^2 . (B) The first foliage leaf of a plant expressing histone H2B-tdTomato was treated with PBS after fixation (upper panels) or cleared using TOMEI-II (lower panels). Confocal optical sections were arranged from the adaxial surface to the abaxial surface. Pink arrows indicate guard cells. (C) The first foliage leaf of a plant expressing histone H2B-tdTomato (magenta) was stained with Calcofluor White (cyan). Dotted lines indicate the outline of vascular veins. (D) Nuclei and cell membranes were visualized with Histone H2B-GFP (green) and LTI6b-tdTomato (magenta), respectively, in a root-knot 6 days post-infection. (E) A three-dimensional image of a root-knot was constructed with FluoRender. Scale bars correspond to 25 μm (D) and 50 μm (B, C).

Fig. 5 Analysis of DNA content and cell volume in transparent giant cells cleared with TOMEI. (A) Cell walls and nuclei in giant cells were stained with Calcofluor White (magenta) and SYBR Green I (green), respectively. Giant cells were cleared with TOMEI-II. A dashed line indicates the giant cell outline. Scale

bar corresponds to 15 μm . (B) Relationship between DNA content and cell volume of root-knot giant cells.

r_s represents the Spearman rank correlation coefficient value ($n = 10$).

Supplementary Fig. S1 Comparison of TOMEI with a previously developed clearing method. The Warner et al. (2014) method (A) and TOMEI (B) were used to treat *A. thaliana* leaves. Sample preparation with the Warner et al. method required 1 week, whereas with TOMEI it was completed in 3 h.

Supplementary Fig. S2 *O. sativa* leaf treated using TOMEI. The *O. sativa* leaf was incubated in clearing solution for 0 min (A) or 40 min (B) and became obviously transparent. These samples were fixed before saturation of the clearing solution.

Supplementary Fig. S3 Autofluorescence of *O. sativa* leaf excited at 405 nm. These images were illuminated and captured at 405 nm from a leaf of *O. sativa* cleared with TOMEI-I without prior staining. Scale bar corresponds to 50 μm .

Supplementary Fig. S4 *O. sativa* leaf stained with DAPI. An *O. sativa* leaf was stained with DAPI and then cleared using TOMEI-I. These images were obtained by confocal microscopy from the adaxial

epidermis to the abaxial epidermis. Scale bar corresponds to 50 μm .

Supplementary Fig. S5 Three-dimensional images of cleared flower stalk and leaf buds reconstructed using two-photon microscopy. A flower stalk (A, B) and leaf buds (C, D) of *A. thaliana* were stained with DAPI and observed using two-photon microscopy. (A) A transparent flower stalk using TOMEI-I was observed using two-photon microscopy. The diameter of the X–Z section is 350 μm . Dashed lines show each axis: blue, X-axis; yellow, Y-axis; green, Z-axis. (B) Optical X–Y section at 175 μm of a flower stalk using two-photon microscopy. Scale bar corresponds to 50 μm . (C) Image of a single optical section of a leaf bud in the shoot apical region. Scale bar corresponds to 25 μm . The pink arrow indicates aligned chromosomes in a mitotic cell at metaphase. (D) Three-dimensional image of the cleared leaf primordium reconstructed with images from two-photon microscopy. A blue arrow indicates a leaf primordium.

Supplementary Fig. 6 Analysis of the signal intensity of fluorescent proteins after TOMEI-II. The fluorescence intensity of H2B-tdTomato in nuclei of guard cells was measured after 0, 24, 48 and 72 h. The fluorescence intensity was normalized to that of PBS-treated samples at the same time-point.

Supplementary Fig. S7 Adaptation of TOMEI for use in conjunction with a yellow fluorescent protein in

A. thaliana leaves. A leaf from a plant expressing histone H2B-YFP was treated using TOMEI-II. Confocal optical sections were arranged from the adaxial surface to the abaxial surface. Dotted lines indicate the outline of vascular veins. Arrowheads show nuclei of guard cells. Scale bar corresponds to 50 μm .

Supplementary Fig. S8 Adaptation of TOMEI for clearing of *A. thaliana* root. A root from a plant expressing histone H2B-GFP (green) and LTI6b-tdTomato (magenta) was stained with DAPI (cyan). The root was cleared with TOMEI-II. The upper panels are optical longitudinal sections and the lower panels are optical transverse sections captured in the plane indicated by dotted line in the upper panel. Scale bar corresponds to 25 μm .

Supplementary Fig. S9 Analysis of DNA content and cell volume in transparent giant cells expressing H2B-GFP and LTI6b-tdTomato cleared with TOMEI-II. The nuclei were visualized by H2B-GFP and the cell membranes by LTI6b-tdTomato in giant cells cleared with TOMEI-II. The DNA amount is proportional to the fluorescence intensity of H2B-GFP. The relationship between DNA content and cell volume of root-knot giant cells can be analyzed based on protein fluorescence intensity. r_s denotes the Spearman rank correlation coefficient ($n = 9$).

Supplementary Mov. S1 Stack of optical sections of a cleared leaf of *A. thaliana* stained with DAPI. A first foliage leaf was stained with DAPI and then cleared using TOMEI-I. Confocal optical sections were arranged from the adaxial surface to the abaxial surface.

Supplementary Mov. S2 Stack of optical sections of a cleared leaf of *O. sativa* stained with SYBR Green I. A leaf blade was stained with SYBR Green I and then cleared using TOMEI-I. Confocal optical sections were arranged from the adaxial surface to the abaxial surface.

Supplementary Mov. S3 Stack of optical sections of a cleared root knot of *A. thaliana* stained with SYBR Green I. A root-knot induced by *M. incognita* infection was stained with SYBR Green I and then cleared using TOMEI-I. Confocal optical sections were arranged from the surface of the root knot to giant cells.

Supplementary Mov. S4 Stack of optical sections of a cleared flower stalk of *A. thaliana* stained with DAPI. A flower stalk was stained with DAPI and then cleared using TOMEI-I. Confocal optical sections were arranged from the epidermis to the central pith.

Supplementary Mov. S5 Stack of optical sections of a cleared flower bud of *A. thaliana* stained with

DAPI. A stage 9 flower bud was stained with DAPI and then cleared using TOMEI-I. Confocal optical sections were arranged from the outer surface of sepals to the gynoecium.

Supplementary Mov. S6 Stack of optical sections of a cleared first true leaf of *A. thaliana* expressing

H2B-tdTomato. A first foliage leaf was cleared using TOMEI-II. Confocal optical sections were arranged from the adaxial surface to the abaxial surface.

For Peer Review

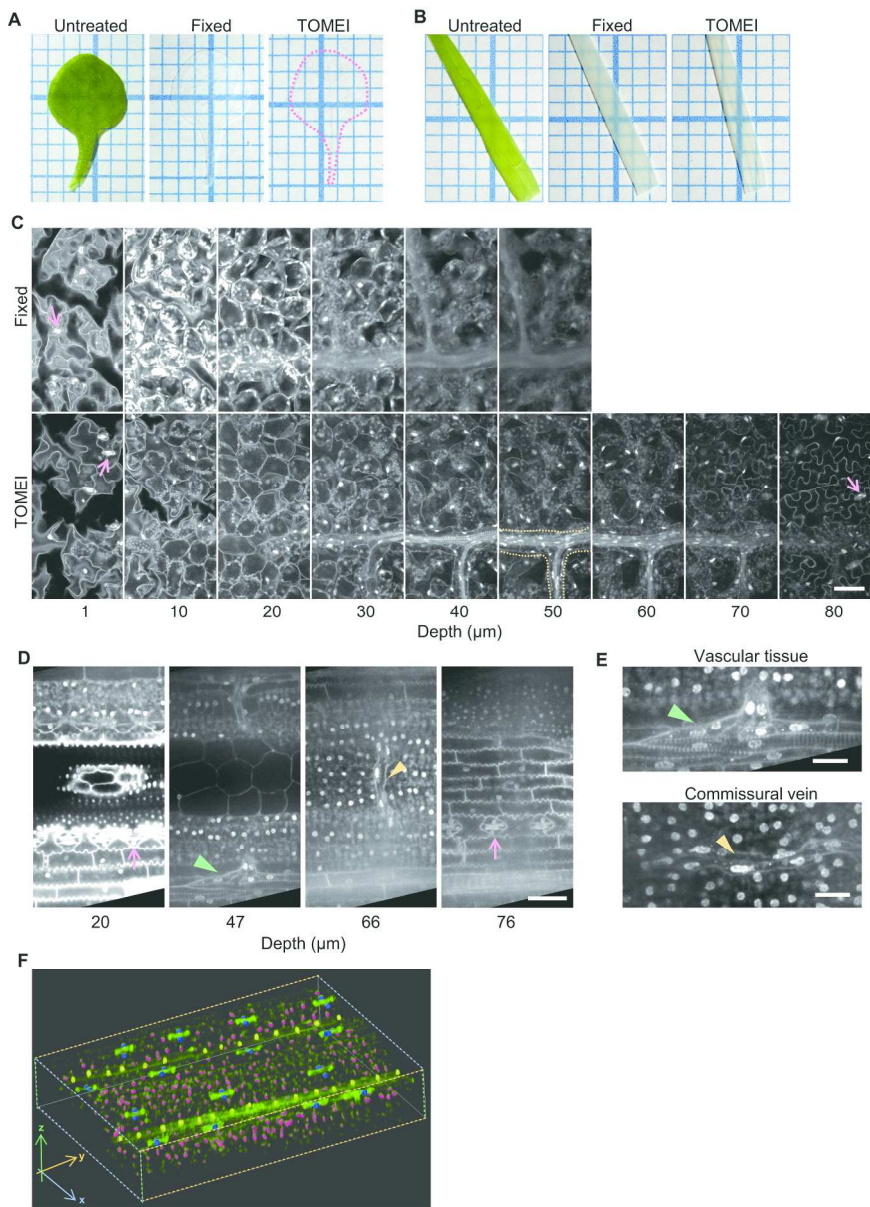


Figure 1. Imaging of *A. thaliana* and *O. sativa* leaves cleared using TOMEI. 201x277mm (300 x 300 DPI)

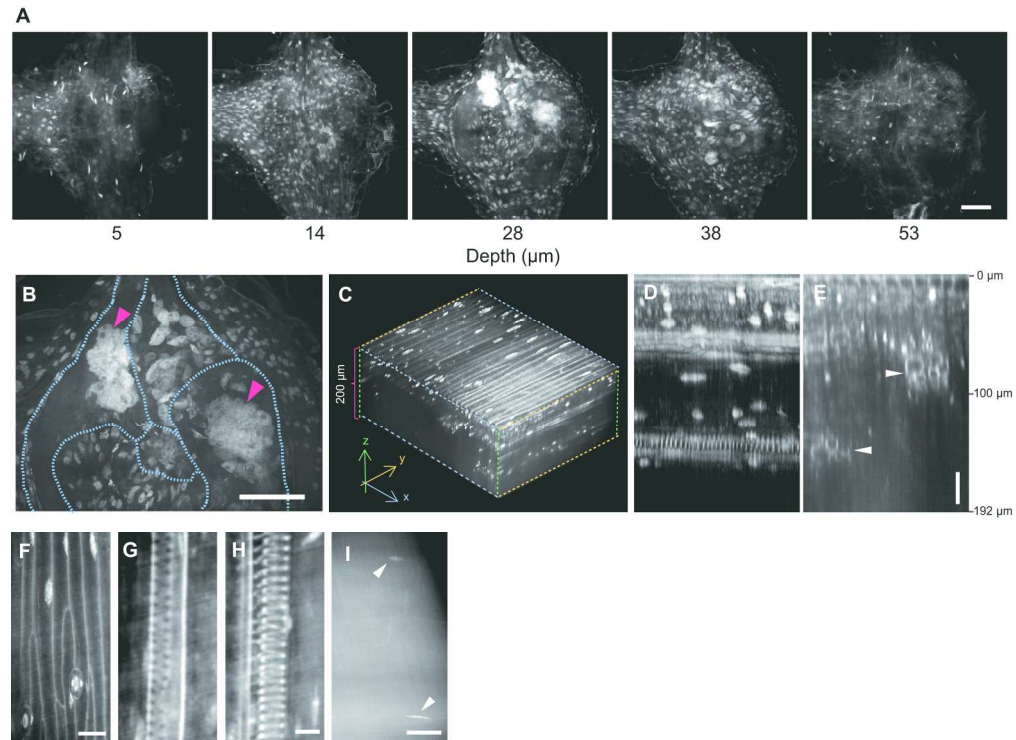


Figure 2. Imaging of *A. thaliana* root-knots and flower stalks cleared using TOMEI.
208x153mm (300 x 300 DPI)

Review

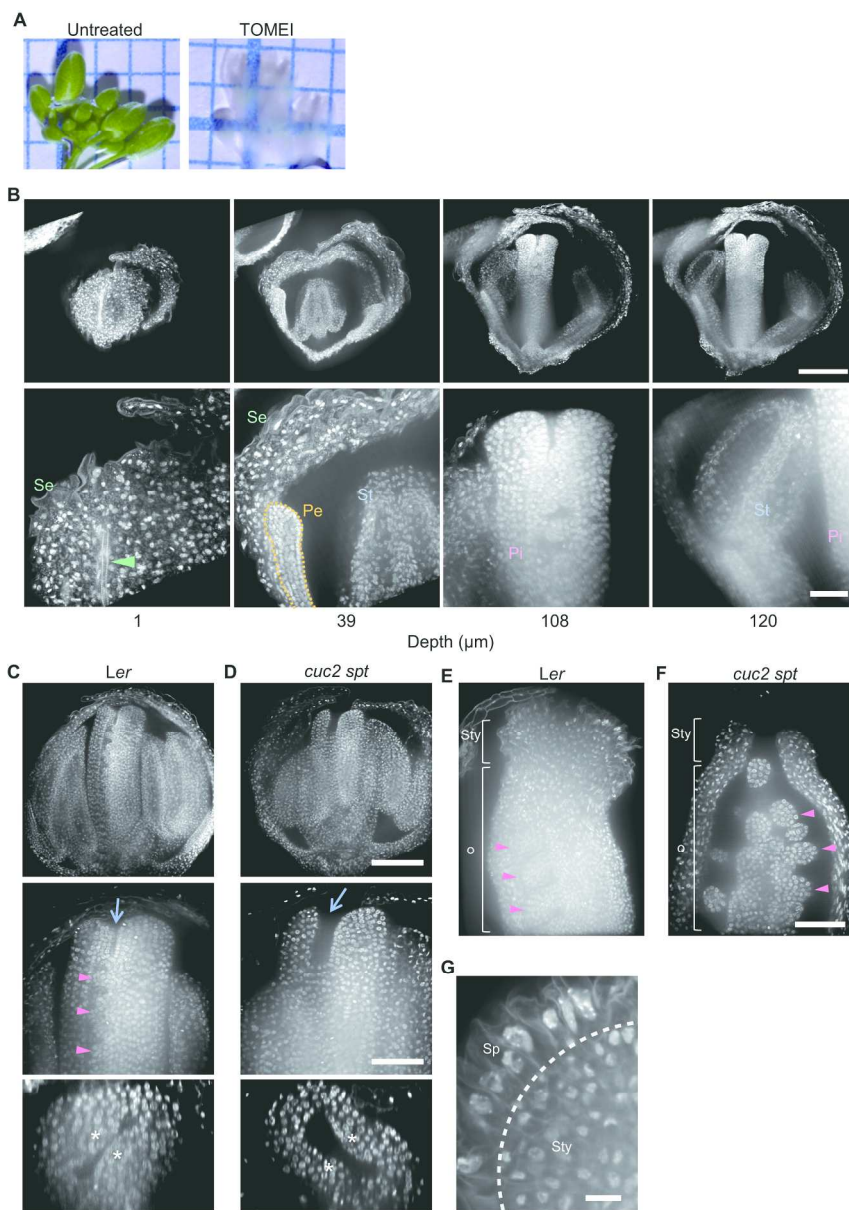


Figure 3. Imaging of *A. thaliana* flower buds cleared using TOMEI. 192x271mm (300 x 300 DPI)

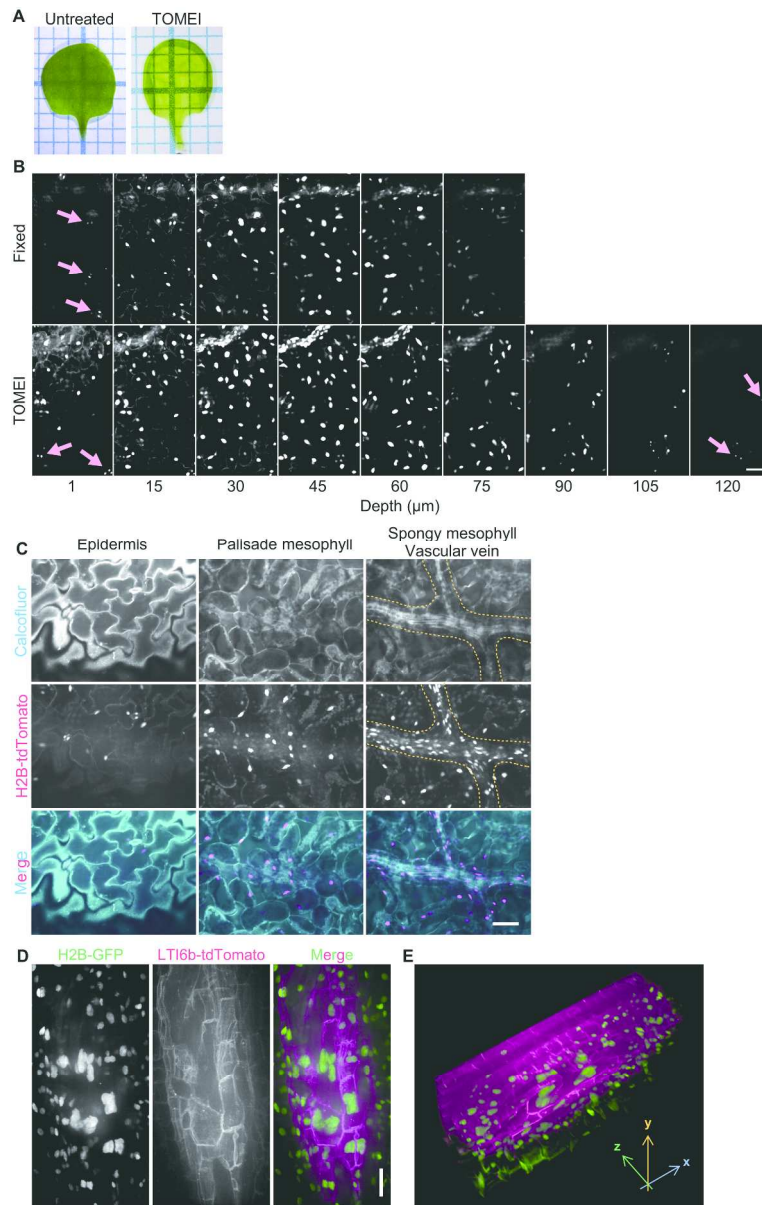


Figure 4. Imaging of fluorescent proteins in *A. thaliana* organs cleared using TOMEI.
187x295mm (300 x 300 DPI)

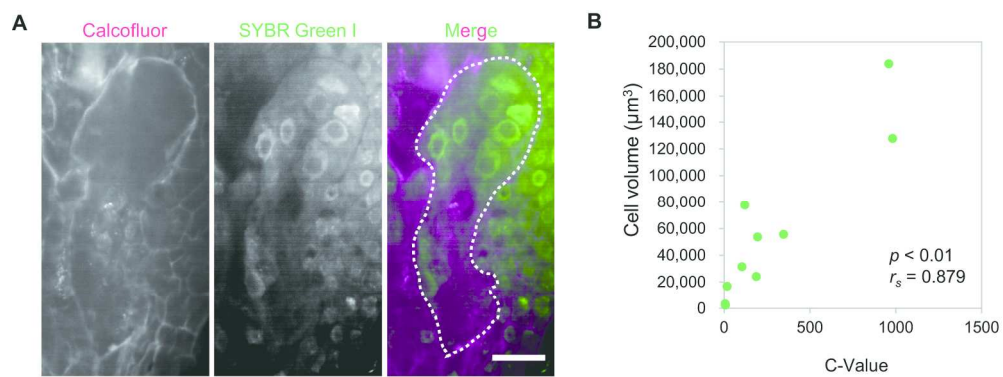


Figure 5. Analysis of DNA content and cell volume in transparent giant cells cleared with TOMEI.
199x75mm (300 x 300 DPI)

Peer Review